Supporting Information for:

Size Selective Incorporation of Gold Nanoparticles in Diblock Copolymer Vesicle Wall

Jiangping Xu[†‡], Han Yuanyuan[†], Jie Cui[†], Wei Jiang*[†]

†State Key Laboratory of Polymer Physics and Chemistry, Changchun Institute of Applied Chemistry, Chinese Academy of Sciences, Changchun 130022, P. R. China

‡University of Chinese Academy of Sciences, Beijing 100049, P. R. China

* Corresponding author, Email address: wjiang@ciac.jl.cn

S1. Additional Experimental Details:

S1.1. Synthesis of $Au_{2.0}R$, $Au_{5.5}R$ and $Au_{1.7}S$

For $Au_{2.0}R$, the traditional Brust two phase method was used.[1] The preparation technique was as follows. An aqueous solution of $HAuCl_4 \cdot 3H_2O$ (0.30 mL, 30 mM) was mixed with a solution of TOAB in toluene (0.80 mL, 50 mM). The mixture was vigorously stirred until all the $HAuCl_4$ was transferred into the organic layer and 1-dodecanethiol (2 mg) was then added to the organic phase. A freshly prepared aqueous solution of $NaBH_4$ (0.25 mL, 0.4 M) was slowly added with vigorous stirring. After further stirring for 3 h the organic phase was separated and mixed with 10 ml ethanol to remove excess 1-dodecanethiol. The $Au_{2.0}R$ was separated by centrifugation and washed by ethanol for 3 times. The final product was dissolved in chloroform and stored at −20 °C. The diameter of the AuNP core is ~2.0 nm (estimated by TEM).

For $Au_{5.5}R$, a modified Brust method introduced by Korgel was used.[2] An aqueous solution of $HAuCl_4 \cdot 3H_2O$ (0.60 mL, 30 mM) was mixed with a solution of TOAB in toluene (0.40 mL, 200 mM). and the mixture was stirred for 1 h. The aqueous phase was discarded. An aqueous of NaBH4 (0.50 mL,

0.4 M) was then added to the organic solution. This mixture was stirred for 3 h. The aqueous phase was then discarded. 1-dodecanethiol (2 mg) was added to the organic phase and the mixture was stirred for 1 h. The crude product was precipitated and washed by ethanol for 3 times. The final product was dissolved in chloroform and stored at −20 °C. The core diameter is ~5.5 nm.

For $Au_{1.7}S$, the Brust two phase method was used.[1, 3] The procedure was the same as it of the synthesis of $Au_{2.0}R$, except of the 1-dodecathiol was replaced by PS_{2k}-SH (18 mg). In a typical purification procedure, $Au_{1.7}S$ were washed with methanol twice to remove TOAB and the precipitate was dissolved in chloroform. Followed by methanol addition to induce NPs precipitation, the precipitate was kept overnight at −20 °C. Then, $Au_{1.7}S$ were separated by centrifugation (10,000 rpm, 20 min). Repeated precipitation-centrifugation procedure (5 times) was conducted until no unbound PS-HS was left, confirmed by Infrared analysis.[4] Finally, $Au_{1.7}S$ was dispersed in chloroform and stored at −20 °C.

S1.2. Synthesis of $Au_{3.5}S$, $Au_{6.2}S$ and $Au_{9.0}S$

The 3.5 nm, 6.2 nm, and 9.0 nm AuNPs were synthesized by seeding growth method.[5] Details were described in the literatures and needed not be repeated here. The citrate-stabilized (3.5 nm) or CTAB-stabilized (6.2 nm and 9.0 nm) NPs were used as the starting material. The aqueous solution of AuNPs was added to equal volume THF solution of PS_{2k}-SH (mole ratio Au:SH=1:0.3). Followed by ultrasonic treatment for 3 h and incubation for 24 h.[3, 6] Subsequently, PS coated AuNPs were separated centrifugation (10,000 rpm, 10 min). Then, similar procedure as the synthesis of $Au_{1.7}S$ was employed to separate PS-coated AuNPs with unbound PS_{2k}-SH and residual surfactant. Furthermore, a second PS-grafting procedure was conducted. PS_{2k}-SH (mole ratio Au:SH=1:0.15) was added to the PS-coated AuNPs THF solution, followed by the same ultrasonic treatment, incubation and purification process as

carried out above. AuNPs with high grafting density were thus obtained (see **Table S1**). NPs core diameter obtained from TEM image analysis was used to calculate the average surface area per NP. Weight fractions of polymer ligands were measured by thermal gravimetric analysis (TGA). PS graft density on the NP surface was estimated based on average particle size from TEM images and the TGA results (see **Table S1**), assuming ρ_{Au} = 19.3 g cm^{-3} and ρ_{PS} = 1.05 g cm^{-3}.

S2. Theory and Simulation Details

In the SCFT, we consider a single polymer chain placed in a set of effective chemical potential fields $\omega_I(\vec{r})$ (I=A, B, P and S) provided by all other components. These chemical potential fields are conjugated to corresponding segment density fields $\phi_I(\vec{r})$. In the canonical ensemble, the dimensionless free energy of the system is given by

$$\begin{aligned} F = & -f_D \ln(\frac{Q_D}{Vf_D}) - \frac{f_G}{(\alpha+\sigma\beta)} \ln(\frac{Q_G}{Vf_G}) - Nf_S \ln(\frac{Q_S}{Vf_S}) \\ & -\frac{1}{V}\int d\vec{r}[\sum_I \omega_I(\vec{r})\phi_I(\vec{r}) + \eta(\vec{r})(1-\sum_I \phi_I(\vec{r}))] \\ & +\frac{1}{V}\int d\vec{r}\sum_{I\neq J}\chi_{IJ}N\phi_I(\vec{r})\phi_J(\vec{r}) \end{aligned} \quad \text{(S1)}$$

Where χ_{IJ} is the Flory-Huggins interaction parameter between components I and J. $\eta(\vec{r})$ is the Lagrange multiplier arising from the incompressibility condition. Q_D, Q_G and Q_S are the partition function of a single polymer chain, a polymer-grafted nanoparticle and a solvent, respectively. In Eq. S1, the first four terms are the contributions of entropy to the total free energy *F*, while the last term is the contribution of enthalpy to *F*.

For a single polymer chain, $Q_D = \int d\vec{r} q_D(\vec{r},1)$, where $q_D(\vec{r},s)$ is the end-segment distribution function that gives the probability of finding segment *s* at position $\vec{r}$. The single polymer chain is

parameterized with the variable *s*, which increases from 0 to 1. With the use of flexible Gaussian model, the end-segment distribution function $q_{\mathrm{D}}(\vec{r},s)$ satisfies the modified diffusion equation

$$\frac{\partial q_{\mathrm{D}}(\vec{r},s)}{\partial s}=\nabla^2 q_{\mathrm{D}}(\vec{r},s)-\omega(\vec{r},s)q_{\mathrm{D}}(\vec{r},s) \tag{S2}$$

Where $\omega(\vec{r},s)$ is $\omega_{\mathrm{A}}(\vec{r},s)$ when $0<s<f_{\mathrm{A}}$ and $\omega_{\mathrm{B}}(\vec{r},s)$ when $f_{\mathrm{A}}<s<1$. The initial condition is $q_{\mathrm{D}}(\vec{r},0)=1$. Because the two ends of AB diblock copolymer are different, a second end-segment distribution function $q_{\mathrm{D}}^{+}(\vec{r},s)$ is needed. $q_{\mathrm{D}}^{+}(\vec{r},s)$ also satisfies Eq. S2. Except that $\omega(\vec{r},s)$ is $\omega_{\mathrm{B}}(\vec{r},s)$ when $0<s<f_{\mathrm{B}}$ and $\omega_{\mathrm{A}}(\vec{r},s)$ when $f_{\mathrm{B}}<s<1$

For the homopolymer A grafted on the nanoparticle, the end-segment distribution function $q_{\mathrm{G}}(\vec{r},s)$ satisfies

$$\frac{\partial q_{\mathrm{G}}(\vec{r},s)}{\partial s}=\beta\nabla^2 q_{\mathrm{G}}(\vec{r},s)-\beta\omega_{\mathrm{A}}(\vec{r},s)q_{\mathrm{G}}(\vec{r},s) \tag{S3}$$

The initial condition is $q_{\mathrm{G}}(\vec{r},0)=1$. The second end-segment distribution function $q_{\mathrm{G}}^{+}(\vec{r},s)$ satisfies Eq. S3 but with the initial condition of $q_{\mathrm{G}}^{+}(\vec{r},0)=\exp[-\alpha\omega_{\mathrm{P}}(\vec{r},s)]q_{\mathrm{G}}(\vec{r},1)^{\sigma-1}$. In terms of $q_{\mathrm{G}}(\vec{r},1)$, the partition function of polymer-grafted nanoparticle can be expressed as $Q_{\mathrm{G}}=\int d\vec{r}\,\exp[-\alpha\omega_{\mathrm{P}}(\vec{r})]q_{\mathrm{G}}(\vec{r},1)^{\sigma}$. For solvent S, the partition function is generally expressed as $Q_{\mathrm{S}}=\int d\vec{r}\cdot\exp[-\omega_{\mathrm{S}}(\vec{r})/N]$.

In terms of these partition functions and end-segment distribution functions, the local densities of each component is obtained by

$$\phi_{\mathrm{A}}(\vec{r})=\frac{f_{\mathrm{D}}V}{Q_{\mathrm{D}}}[\int_0^{f_{\mathrm{A}}} ds\cdot q_{\mathrm{D}}(\vec{r},s)q_{\mathrm{D}}^{+}(\vec{r},1-s)] \tag{S4}$$

$$\phi_{\mathrm{B}}(\vec{r}) = \frac{f_{\mathrm{D}}V}{Q_{\mathrm{D}}}[\int_{f_{\mathrm{A}}}^{1} ds \cdot q_{\mathrm{D}}(\vec{r},s)q_{\mathrm{D}}^{+}(\vec{r},1-s)] + \frac{f_{\mathrm{G}}\sigma\beta V}{(\alpha+\sigma\beta)Q_{\mathrm{G}}}\int_{0}^{1} ds \cdot q_{\mathrm{G}}(\vec{r},s)q_{\mathrm{G}}^{+}(\vec{r},1-s)] \tag{S5}$$

$$\phi_{\mathrm{P}}(\vec{r}) = \frac{f_{\mathrm{G}}\alpha V}{(\alpha+\sigma\beta)Q_{\mathrm{G}}}\exp[-\alpha\omega_{\mathrm{P}}(\vec{r})]q_{\mathrm{G}}(\vec{r},1)^{\sigma} \tag{S6}$$

$$\phi_{\mathrm{S}}(\vec{r}) = \frac{f_{\mathrm{S}}V}{Q_{\mathrm{S}}}\exp[-\omega_{\mathrm{S}}(\vec{r})/N] \tag{S7}$$

From the equilibrium condition, the minimization of free energy with respective to density and Lagrange multiplier (i.e., $\delta F/\delta\phi = \delta F/\delta\eta = 0$), we can obtain another five equations:

$$\omega_{\mathrm{A}}(\vec{r}) = \chi_{\mathrm{AB}}N(\phi_{\mathrm{B}}(\vec{r}) - f_{\mathrm{B}}) + \chi_{\mathrm{AP}}N(\phi_{\mathrm{P}}(\vec{r}) - f_{\mathrm{P}}) + \chi_{\mathrm{AS}}N(\phi_{\mathrm{S}}(\vec{r}) - f_{\mathrm{S}}) + \eta(\vec{r}) \tag{S8}$$

$$\omega_{\mathrm{B}}(\vec{r}) = \chi_{\mathrm{AB}}N(\phi_{\mathrm{A}}(\vec{r}) - f_{\mathrm{A}}) + \chi_{\mathrm{BP}}N(\phi_{\mathrm{P}}(\vec{r}) - f_{\mathrm{P}}) + \chi_{\mathrm{BS}}N(\phi_{\mathrm{S}}(\vec{r}) - f_{\mathrm{S}}) + \eta(\vec{r}) \tag{S9}$$

$$\omega_{\mathrm{P}}(\vec{r}) = \chi_{\mathrm{AP}}N(\phi_{\mathrm{A}}(\vec{r}) - f_{\mathrm{A}}) + \chi_{\mathrm{BP}}N(\phi_{\mathrm{B}}(\vec{r}) - f_{\mathrm{B}}) + \chi_{\mathrm{PS}}N(\phi_{\mathrm{S}}(\vec{r}) - f_{\mathrm{S}}) + \eta(\vec{r}) \tag{S10}$$

$$\omega_{\mathrm{S}}(\vec{r}) = \chi_{\mathrm{AS}}N(\phi_{\mathrm{A}}(\vec{r}) - f_{\mathrm{A}}) + \chi_{\mathrm{BS}}N(\phi_{\mathrm{B}}(\vec{r}) - f_{\mathrm{B}}) + \chi_{\mathrm{PS}}N(\phi_{\mathrm{P}}(\vec{r}) - f_{\mathrm{P}}) + \eta(\vec{r}) \tag{S11}$$

$$\phi_{\mathrm{A}}(\vec{r}) + \phi_{\mathrm{B}}(\vec{r}) + \phi_{\mathrm{P}}(\vec{r}) + \phi_{\mathrm{S}}(\vec{r}) = 1 \tag{S12}$$

Equations S2-S12 can be solved self-consistently in the real-space SCFT by the combinatorial screening algorithm proposed by Drolet and Fredrickson.[7-9] In this paper, the numerical simulations were carried out in 3D cubic lattice with a volume of $V = 50\times50\times100$. Periodic boundary conditions were imposed in all three directions and the grid size we chose was $\Delta x = 0.35$. To obtain vesicles in simulations, the interaction parameters between different components were set to be $\chi_{\mathrm{AS}}N$=22, $\chi_{\mathrm{BS}}N$=−16, $\chi_{\mathrm{PS}}N$=100 And $\chi_{\mathrm{AB}}N$=$\chi_{\mathrm{AP}}N$=$\chi_{\mathrm{BP}}N$=16 .The simulation was carried out until the morphologies were stable. The same initial fluctuation amplitude in the order of 10^{-3} was used in our work.

S3. Supporting Data

S3.1. Characterization of the Au_xR and Au_xS

The core diameters of the AuNPs were examined by TEM (JEOL JEM-1011, 100kV) and the graft density was measured by TGA (TA, Q50).

Table S1. The characterization of the ligands coated gold nanoparticles.

AuNPs	D_{core} (nm)[a]	$D_{core+shell}$ (nm)[b]	$w_{ligands}$ (%)[c]	Graft Density (chain/nm^2)[d]
$Au_{2.0}R$	2.0	3.4	25	6.42
$Au_{5.5}R$	5.5	6.9	15	9.35
$Au_{1.9}S$	1.9	6.7	70	4.29
$Au_{3.5}S$	3.5	10.4	58	4.67
$Au_{6.2}S$	6.2	12.8	30	2.57
$Au_{9.0}S$	9.0	16.2	21	2.32

Note: a. The diameters of the AuNP cores were obtained from TEM images; b. The $D_{core+shell}$ includes the size of the core and the ligand thickness of the AuNPs. For Au_xR, the ligand thickness measured by TEM is 1.4 nm, which is the surface-to-surface distance of the closely stacked Au_xR. Thus, the $D_{core+shell}$ of the Au_xR is the sum of D_{core} and 1.4 nm. For Au_xS, $D_{core+shell}$ is calculated according to the following equation (see below, Eq. S14); c. $w_{ligands}$ is the weight fraction of the ligands to the Au_xR or Au_xS, obtained from TGA; d. The graft density was obtained based on the results of TGA and TEM.

The equation used to calculate the $D_{core+shell}$ of Au_xS is

$$\frac{\rho_{PS}[\frac{4}{3}\pi(\frac{D_{core+shell}}{2})^3-\frac{4}{3}\pi(\frac{D_{core}}{2})^3]}{\rho_{PS}[\frac{4}{3}\pi(\frac{D_{core+shell}}{2})^3-\frac{4}{3}\pi(\frac{D_{core}}{2})^3]+\rho_{Au}\frac{4}{3}\pi(\frac{D_{core}}{2})^3}=w_{PS} \quad \text{(S13)}$$

Eq.S13 can be simplified as

$$D_{\text{core+shell}} = D_{\text{core}}\left(\frac{\rho_{\text{Au}} w_{\text{PS}}}{\rho_{\text{PS}} w_{\text{Au}}} + 1\right)^{1/3}, \quad \text{(S14)}$$

Where ρ_{PS} = 1.05 g cm^{-3} is the density of PS solid, ρ_{Au} = 19.3 g cm^{-3} is the density of gold, w_{PS} is the weight fraction of PS obtained by TGA, w_{Au} is the weight fraction of AuNPs cores, $w_{\text{Au}} = 1 - w_{\text{PS}}$. As the D_{core} can be measured by TEM, the $D_{\text{core+shell}}$ can be figured out according to Eq.S14.

S3.2. Self-assembly of PS_{144}-*b*-PAA_{22} in THF/water

Neat PS_{144}-*b*-PAA_{22} (2 mg) was dissolved in 0.5 mL THF, then 0.125 mL water was dropwise added to the solution. The equilibrium morphology of the aggregates was vesicle (Figure S1c). The kinetics of the vesicle formation was *ex situ* studied by TEM, as shown in Figure S1. At the early stage, the main morphology was sphere. As the stirring time extended, cavities appeared in the core of the hybrid spherical micelles (Figure S1b). They were the intermediate structures of the swell mechanism of sphere-to-vesicle transition, which was described in detail by He and coworkers. After being stirred for 3 days, all of the aggregates were vesicles (Figure 1Sc).

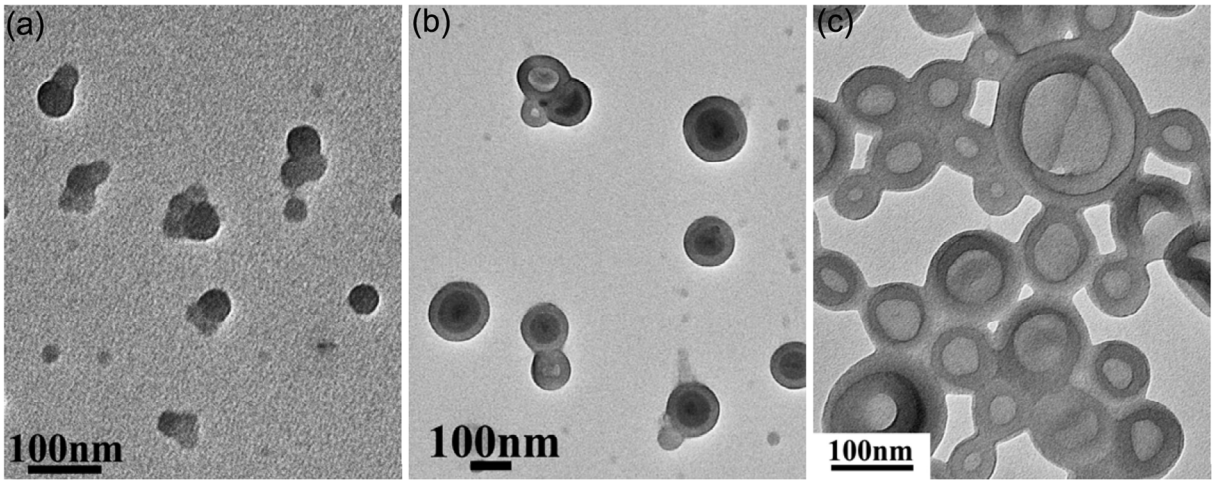

Figure S1. Neat PS_{144}-*b*-PAA_{22} self-assemble into vesicles in THF/water (4:1, v/v) binary mixed

solvents. Morphologies of the aggregates at different stages, (a) 3h, (b) 1 day, (c) 3 days, are obtained by TEM

S3.3. Cooperative self-assembly of Au_xS and PS_{356}-*b*-PEO_{148} in DMF/water

In the cooperative self-assembly of Au_xS and diblock copolymer, the volume fraction of Au_xS (φ_{Au_xS}) is estimated as follows,

$$\varphi_{Au_xS} = \frac{V_{Au_xS}}{V_{Au_xS} + V_{PS\ block}}, \quad \text{(S15)}$$

where V_{Au_xS} is the volume of Au_xS, $V_{PS\ block}$ is the volume of the PS block of diblock copolymer. Usually the TEM images show the morphology of the phase with high electron density, the low-electron-density area is nearly invisible. For example, the PS cores of the assemblies of PS-*b*-PAA or PS-*b*-PEO can be seen, but the PAA or PEO shells are invisible. As a result, we defined such a φ_{Au_xS} to give a visualized information from the TEM images.

The requisite amount (φ_{Au_xS} = 5.4 %) of the AuNPs chloroform solution was added to a vial and dried in nitrogen flow. DMF solution of PS_{356}-*b*-PEO_{148} (4 mg mL^{-1}, 0.50 mL) was then added to the vial. After being stirred for 10 min, 0.08 mL water was dropwise added to the mixture. The mixture was stirred at 500 rpm for 2 days at room temperature. The neat PS_{356}-*b*-PEO_{148} can self-assembly into vesicles (wall thickness 33.0 nm, Figure S2a) in DMF/water. The $Au_{1.9}S$ (D_0/d_{w0} = 0.20), $Au_{3.5}S$ (D_0/d_{w0} = 0.32), and $Au_{6.2}S$ (D_0/d_{w0} = 0.39) can be inserted in the vesicle wall (Figure S2b-d). The $Au_{9.0}S$ (D_0/d_{w0} = 0.49) can locate in both vesicle wall and spherical micelle (Figure S2e).

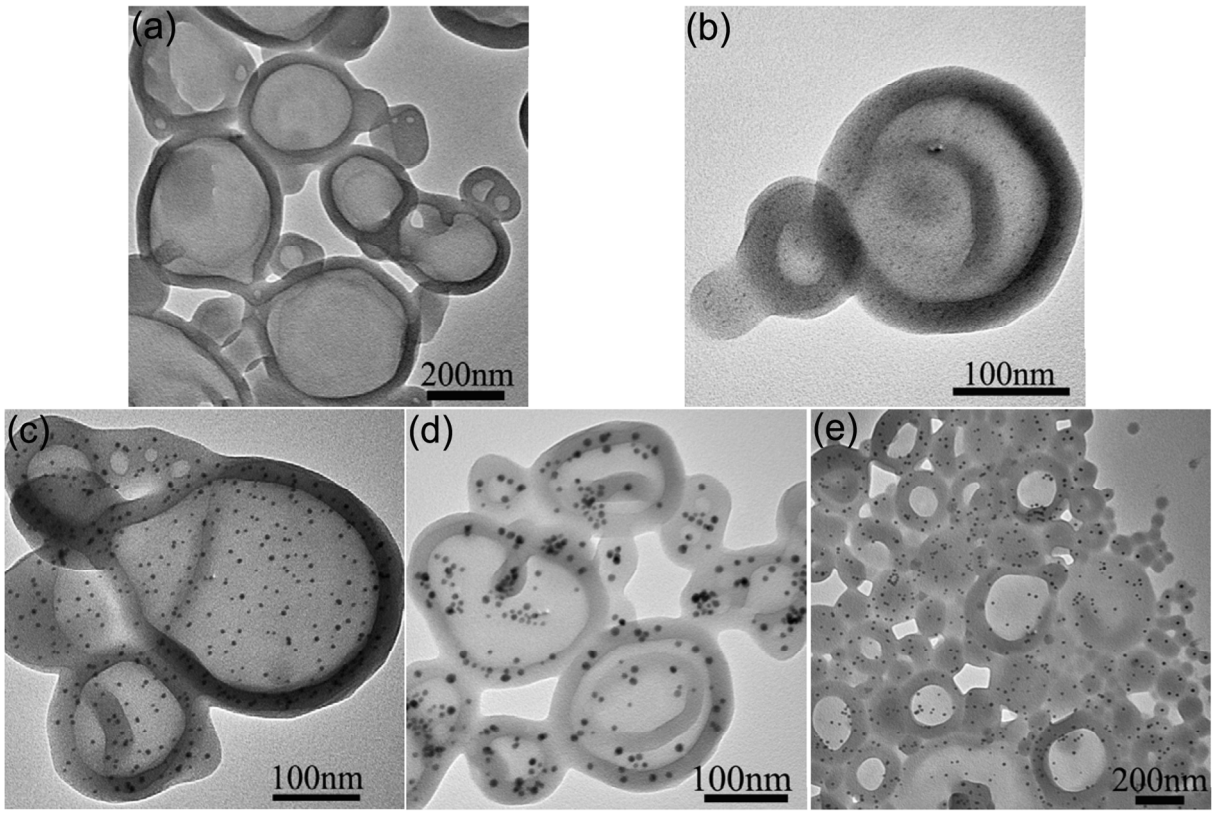

Figure S2. Cooperative self-assembly of Au_xS and PS_{356}-*b*-PEO_{148} in DMF/water. (a) neat PS_{356}-*b*-PEO_{148} can self-assemble into vesicle whose wall thickness d_{w0} = 33.0 nm. (b)-(d) the $Au_{1.9}S$, $Au_{3.5}S$, and $Au_{6.2}S$ can be inserted in the vesicle wall. (e) the $Au_{9.0}S$ can locate in both vesicle wall and spherical micelle.

S3.4. Cooperative self-assembly of Au_xS and PS_{144}-*b*-PAA_{22} in dioxane/water

As demonstrated by Eisenberg et al.,[10] the solvent property played a key role in the stretching degree of the PS block, which determined the thickness of the vesicle wall. Thus, the vesicles self-assembled from the same block copolymer may have different wall thickness in different solvents. We attempted to obtain vesicles in dioxane/water mixture and studied the encapsulation of Au_xS in the vesicle wall. Typically, the requisite amount (φ_{Au_xS} = 5.4 %) of the AuNPs chloroform solution was

added to a vial and dried in nitrogen flow. Dioxane solution of PS_{144}-*b*-PAA_{22} (4 mg mL^{-1}, 0.50 mL) was then added to the vial. After being stirred for 10 min, 0.10 mL water was dropwise added to the mixture. The mixture was stirred at 500 rpm for 2 days at room temperature. The neat PS_{144}-*b*-PAA_{22} can self-assembly into vesicles (wall thickness 23.9 nm, Figure S3a) in dioxane/water. Both the $Au_{1.9}S$ (D_0/d_{w0} = 0.28) and the $Au_{3.5}S$ (D_0/d_{w0} = 0.44) can be inserted in the vesicle wall (Figure S3b, c). However, the $Au_{6.2}S$ (D_0/d_{w0} = 0.54) and the $Au_{9.0}S$ (D_0/d_{w0} = 0.68) can't be encapsulated in the vesicle wall (Figure S3d, e). These results confirm that when $D_0/d_{w0} < 0.50$, the Au_xS can be incorporated in the vesicle wall; when $D_0/d_{w0} > 0.50$, the Au_xS selectively locate in the spherical micelle. Furthermore, we conducted another experiment in which the $Au_{1.9}S$ and $Au_{9.0}S$ simultaneously self-assembled with PS_{144}-b-PAA_{22} in dioxane/water mixture. As shown in Figure S3f, the $Au_{1.9}S$ can locate in both vesicles and spherical micelles, but the $Au_{9.0}S$ selectively stay in the core of spherical micelles.

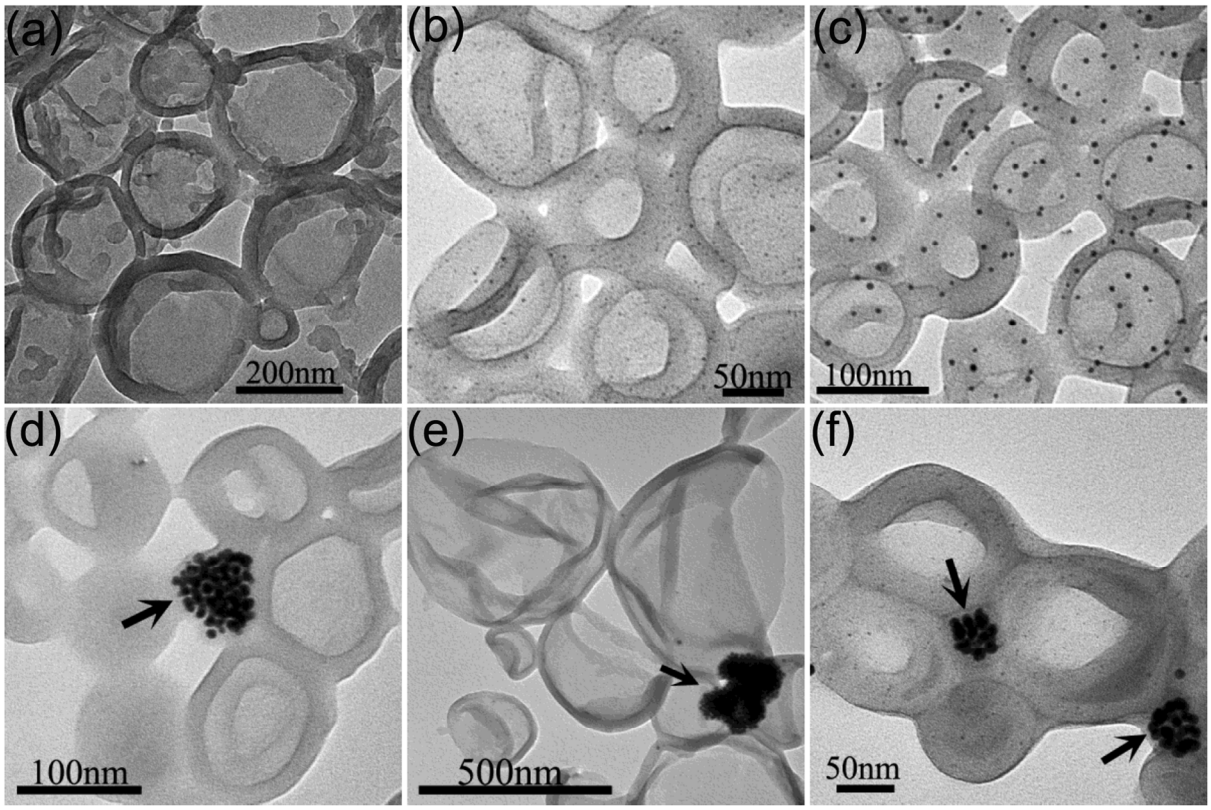

Figure S3. Cooperative self-assembly of Au_xS and PS_{144}-*b*-PAA_{22} in dioxane/water. (a) neat PS_{144}-b-PAA_{22} can self-assemble into vesicle whose wall thickness d_{w0} = 23.9 nm. (b) $Au_{1.9}S$ can be inserted into the wall, D_0/d_{w0} = 0.28; (c) $Au_{3.5}S$ can stably stay in the wall, D_0/d_{w0} = 0.44; (c) $Au_{6.2}S$ can not be inserted in the wall, D_0/d_{w0} = 0.54. They prefer to aggregating in the core of spherical micelle (pointed out by arrows); (d) $Au_{9.0}S$ can't be incorporated in the wall, D_0/d_{w0} = 0.68. They selectively aggregate in the core of spherical micelle (pointed out by arrows); (e) Simultaneously self-assembly of two types of PS-terminated AuNPs, $Au_{1.9}S$ and $Au_{9.0}S$, with PS_{144}-*b*-PAA_{22}. The $Au_{1.9}S$ stay in the vesicle wall, while the $Au_{9.0}S$ selectively locate in the spheres (pointed out by arrows).

S3.5. Cooperative self-assembly of Au_xS and PS_{356}-*b*-PEO_{148} in dioxane/water

The requisite amount (φ_{Au_xS} = 5.4 %) of the AuNPs chloroform solution was added to a vial and

dried in nitrogen flow. Dioxane solution of PS_{356}-*b*-PEO_{148} (4 mg mL^{-1}, 0.50 mL) was then added to the vial. After being stirred for 10 min, 0.10 mL water was dropwise added to the mixture. The mixture was stirred at 500 rpm for 2 days at room temperature. The neat PS_{356}-*b*-PEO_{148} can self-assembly into vesicles (wall thickness 27.9 nm, Figure S4a). Both $Au_{1.9}S$ (D_0/d_{w0} = 0.24) and $Au_{3.5}S$ (D_0/d_{w0} = 0.37) can be incorporated in the vesicle wall (Figure S4b,c). However, only a part of the $Au_{6.2}S$ (D_0/d_{w0} = 0.46) can be inserted in the wall (Figure S4d). Some of them aggregate in the core of spherical micelle. For the $Au_{9.0}S$ (D_0/d_{w0} = 0.58), most of the AuNPs locate in the core of spherical micelle, while few of them can be found in vesicle wall. These results again confirm that when $D_0/d_{w0} < 0.50$, the Au_xS can be incorporated in the vesicle wall; when $D_0/d_{w0} > 0.50$, the Au_xS selectively located in the spherical micelle. Furthermore, hybrid cylindrical micelles and hybrid toroidal micelles with $Au_{9.0}S$ in the core can be found when the $Au_{9.0}S$ co-assemble with PS_{356}-*b*-PEO_{148} in dioxane/water (Figure S4f). This morphological transition is coincident with Lin's work.[11] In their simulation study, transition from vesicle to rod-like micelle induced by the increasing nanoparticle diameter was observed. This morphological change can be attributed to the increase of volume fraction of the hydrophobic core due to the incorporation of the hydrophobic $Au_{9.0}S$.[11]

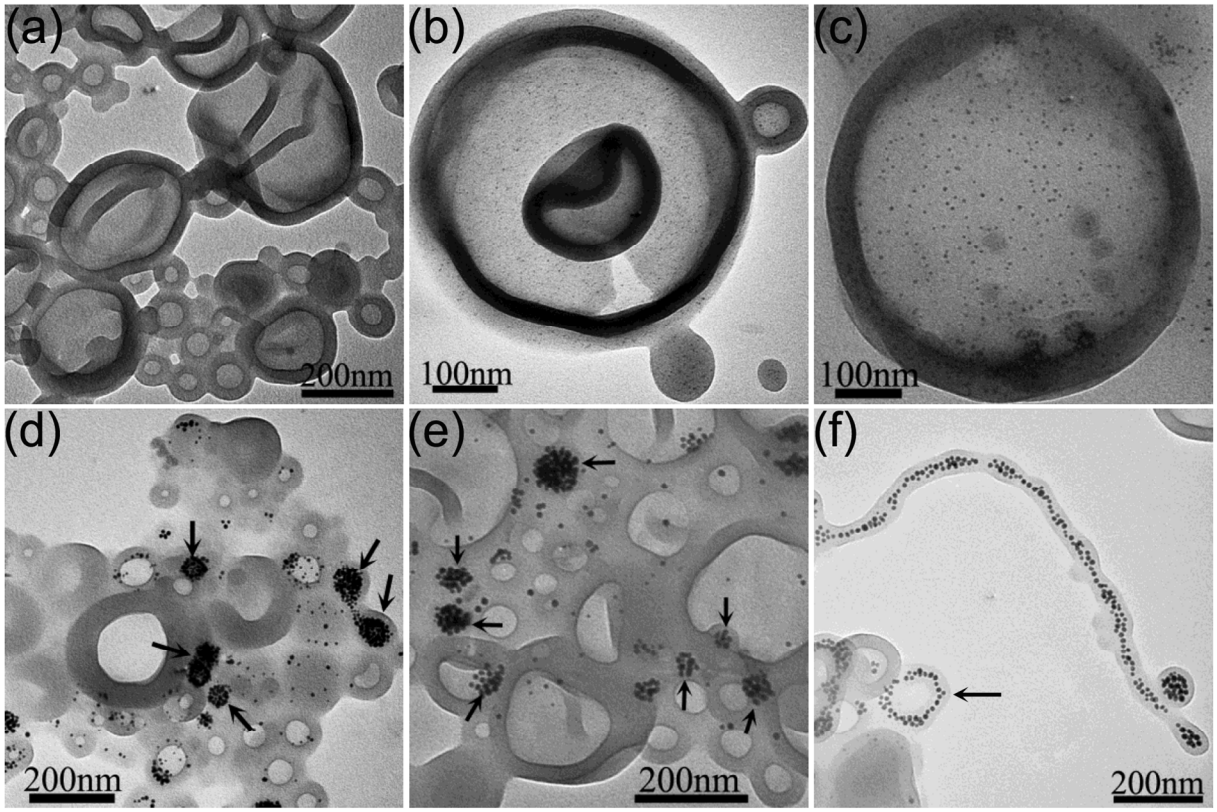

Figure S4. Cooperative self-assembly of Au_xS and PS_{356}-*b*-PEO_{148} in dioxane/water. (a) neat PS_{356}-b-PEO_{148} can self-assemble into vesicle whose wall thickness d_{w0} = 27.9 nm. (b) $Au_{1.9}S$ can be inserted into the wall, D_0/d_{w0} = 0.24; (c) $Au_{3.5}S$ can stably stay in the wall, D_0/d_{w0} = 0.37; (d) $Au_{6.2}S$ can partially be inserted in the wall, D_0/d_{w0} = 0.46. Some of them aggregate in the core of spherical micelle (pointed out by arrows); (e) $Au_{9.0}S$ can't be incorporated in the wall, D_0/d_{w0} = 0.58. They selectively locate in the core of spherical micelle (pointed out by arrows); (f) Hybrid cylindrical micelles and hybrid toroidal micelles (pointed out by arrow) with $Au_{9.0}S$ in the core can be found when the $Au_{9.0}S$ co-assemble with PS_{356}-*b*-PEO_{148} in dioxane/water.

References

(1) Brust, M.; Walker, M.; Bethell, D.; Schiffrin, D. J.; Whyman, R., Synthesis of Thiol-Derivatized

Gold Nanoparticles in a Two-Phase Liquid-Liquid System. *J. Chem. Soc., Chem. Commun.* **1994**, *7*, 801-802.

(2) Smith, D. K.; Goodfellow, B.; Smilgies, D. M.; Korgel, B. A., Self-Assembled Simple Hexagonal AB_2 Binary Nanocrystal Superlattices: SEM, GISAXS, and Defects. *J. Am. Chem. Soc.* **2009**, *131*, 3281-3290.

(3) Li, W. K.; Liu, S. Q.; Deng, R. H.; Zhu, J. T., Encapsulation of Nanoparticles in Block Copolymer Micellar Aggregates by Directed Supramolecular Assembly. *Angew. Chem. Int. Ed.* **2011**, *50*, 5865-5868.

(4) Yockell-Lelièvre, H.; Desbiens, J.; Ritcey, A. M., Two-Dimensional Self-Organization of Polystyrene-Capped Gold Nanoparticles. *Langmuir* **2007**, *23*, 2843-2850.

(5) Jana, N. R.; Gearheart, L.; Murphy, C. J., Seeding Growth for Size Control of 5-40 nm Diameter Gold Nanoparticles. *Langmuir* **2001**, *17*, 6782-6786.

(6) Nie, Z. H.; Fava, D.; Kumacheva, E.; Zou, S.; Walker, G. C.; Rubinstein, M., Self-Assembly of Metal-Polymer Analogues of Amphiphilic Triblock Copolymers. *Nat. Mater.* **2007**, *6*, 609-614.

(7) Drolet, F.; Fredrickson, G. H., Combinatorial Screening of Complex Block Copolymer Assembly with Self-Consistent Field Theory. *Phys. Rev. Lett.* **1999**, *83*, 4317-4320.

(8) Drolet, F.; Fredrickson, G. H., Optimizing Chain Bridging in Complex Block Copolymers. *Macromolecules* **2001**, *34*, 5317-5324.

(9) Fredrickson, G. H.; Ganesan, V.; Drolet, F., Field-Theoretic Computer Simulation Methods for Polymers and Complex Fluids. *Macromolecules* **2002**, *35*, 16-39.

(10) Yu, Y. S.; Zhang, L. F.; Eisenberg, A., Morphogenic Effect of Solvent on Crew-Cut Aggregates of

Apmphiphilic Diblock Copolymers. *Macromolecules* **1998**, *31*, 1144-1154.

(11) Zhang, L.; Lin, J.; Lin, S., Self-Assembly Behavior of Amphiphilic Block Copolymer/Nanoparticle Mixture in Dilute Solution Studied by Self-Consistent-Field Theory/Density Functional Theory. *Macromolecules* **2007**, *40*, 5582-5592.